Available online at www.sciencedirect.com
SCIENCE DIRECT®
Journal of Sound and Vibration 273 (2004) 1047–1062
JOURNAL OF SOUND AND VIBRATION
www.elsevier.com/locate/jsvi

Stability analysis for the flapwise motion of a cantilever beam with rotary oscillation

Jintai Chung[a,*], Duhan Jung[b], Hong Hee Yoo[c]

[a] *Department of Mechanical Engineering, Hanyang University, 1271 Sa-1-dong, Ansan, Kyunggi-do 425-791, South Korea*
[b] *Department of Precision Mechanical Engineering, Hanyang University, 17 Haengdang-dong, Seongdong-ku, Seoul 133-791, South Korea*
[c] *School of Mechanical Engineering, Hanyang University, 17 Haengdang-dong, Seongdong-ku, Seoul 133-791, South Korea*

Received 9 September 2002; accepted 12 May 2003

Abstract

The flapwise motion of a cantilever beam with rotary oscillation is analyzed to investigate the dynamic stability of the beam. The cantilever beam is regarded as a system subjected to parametric excitation because the angular speed of the cantilever beam varies harmonically. To consider the stiffening effect due to the centrifugal force, this study adopts the linear partial differential equation of flapwise motion, which is derived by a modelling method using the stretch deformation instead of the conventional longitudinal deformation. After the partial differential equation is discretized by the Galerkin method, the method of multiple scales is applied. Using this method, the stability of the beam is analyzed for the variations of the oscillating frequency and the maximum angular speed. In addition, to verify the stability results, the time responses of flapwise motion are computed by the generalized-α time integration method.

1. Introduction

It is well known that the lateral stiffness of cantilever beams is influenced by rigid-body motion. For instance, a rotating cantilever beam has larger bending stiffness than a stationary cantilever beam, because rotation yields a stiffening effect due to a centrifugal force. Similarly, when a cantilever beam swings periodically, that is, oscillates about the axis of rotation, the dynamic bending stiffness varies harmonically. Therefore, a cantilever beam with rotary oscillation can be regarded as a parametric excitation system.

*Corresponding author. Tel.: +82-31-400-5287; fax: +82-31-406-5550.
E-mail address: jchung@hanyang.ac.kr (J. Chung).

0022-460X/03/$ - see front matter
doi:10.1016/S0022-460X(03)00521-2

The vibration of a parametrically excited system was introduced by Faraday [1], and fundamental mathematical bases were established in Refs. [2,3]. Stephenson [4] pointed out that a column under the influence of a periodic load might be stable even though the steady value of the load is twice that of the Euler load. Andronov and Leontovich [5] investigated the responses of a straight elastic column to an axial periodic load. The results showed that a column could be unstable if half of the oscillating frequency is close to one of the natural frequencies of the lateral motion. In this sense, a large number of papers regarding problems involving parametric excitations have been published [6–10]. Recently, Wickert and Mote [11] discretized the distributed parameter model using single mode expansion to assess the perturbation solution. Wickert [12] also investigated gyroscopic dynamic systems with unsteady rotation or translation. Pakdemirli and Ulsoy [13] investigated the stability of a string travelling with a time-dependent velocity. Hyun and Yoo [14] studied the dynamic stability of an axially oscillating cantilever beam considering the stiffness variation. Lin and Chen [15] studied the dynamic stability of a rotating composite beam with a constrained damping layer subjected to axial periodic loads. The dynamic stability of a radially rotating beam subjected to base excitation was investigated by Tan et al. [16]. They also analyzed the parametric instability of spinning pretwisted beam subjected to spin speed perturbation [17]. With a few exceptions, most of these studies have addressed the axially oscillating problem.

On the other hand, Yoo et al. [18] analyzed the dynamics of a rotating cantilever beam. They presented a linear modelling method for the dynamic analysis of a flexible beam undergoing overall motion. This modelling method employs hybrid deformation variables (including a stretch variable) along with a special linear strain measure. The advantage of the linear modelling method is to accurately reflect the stiffening effect due to the centrifugal force, which is poorly estimated in the classical linear modelling method [19–21]. Base on this modelling method, Chung and Yoo [22] derived the partial differential equations of motion for a rotating cantilever beam and presented a finite element analysis to investigate the natural frequencies and time responses.

This study investigates the dynamic stability for the flapwise motion of a cantilever beam by using the method of multiple scales [23,24], when the beam oscillates in the rotation direction. Because the angular velocity of the beam is given as a harmonic function of time, the beam can be regarded as a parametrically excited system. To describe the flapwise motion, the linear partial differential equation of flapwise motion derived in Ref. [22] is used. Since the partial differential equation is not only linear but also captures the motion-induced stiffness accurately, the differential equation is adequate for the stability analysis. After the equation is transformed into a dimensionless form, it is discretized by the Galerkin method. Applying the method of multiple scales to the discretized equations, the stability of the beams with rotary oscillation is analyzed for the variations of the oscillating frequency and the maximum angular speed. To verify the results of the stability analysis, the time responses of flapwise motion are computed by the generalized-α time integration method [25].

2. Equation of motion

A cantilever beam oscillating about the rotation axis is shown in Fig. 1 where the angular speed $\Omega(t)$ is given by a harmonic function of time t. The cantilever beam with length L is modelled as

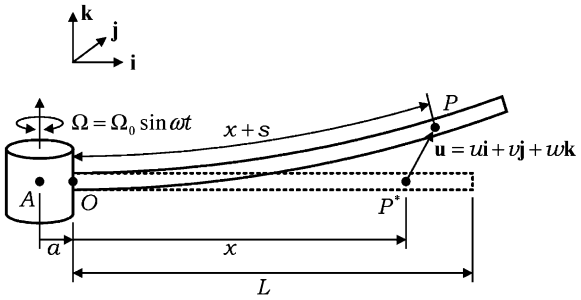

Fig. 1. Configuration of a cantilever beam with rotary oscillation.

the Euler–Bernoulli beam and fixed at point O of a rigid hub with a radius a. The orthogonal unit vectors **i**, **j** and **k** rotate with the hub: **i** is along the beam before deformation, **j** is in the tangential direction of the hub, and **k** is in the direction of the hub axis. In Fig. 1, the straight and curved beams represent the beams before and after deformation. When point P^* moves to point P, the deformation of the beam may be described by the longitudinal deformation u, the chordwise deformation v and the flapwise deformation w, in the directions of **i**, **j** and **k**, respectively. However, this study adopts the stretch deformation s instead of the longitudinal deformation u, because the use of stretch deformation has an advantage over the use of longitudinal deformation, as pointed out in the introduction.

As presented in Ref. [22], the relationship between the stretch, longitudinal, chordwise and flapwise deformations is given by

$$u = s - \frac{1}{2}\int_0^x \left[\left(\frac{\partial v}{\partial \eta}\right)^2 + \left(\frac{\partial w}{\partial \eta}\right)^2\right] \mathrm{d}\eta, \tag{1}$$

where η is a dummy variable. The equations of motion for a cantilever beam undergoing overall motion may be obtained by using s, v and w instead of u, v and w. The detailed procedures to derive the equations of motion can be found in Ref. [22]. The equations of streching and chordwise motions are coupled to each other while the equation of flapwise motion is not coupled with the other equations. Therefore, the equation of flapwise motion can be solved independently of the other equations.

Only the flapwise motion described by w is considered in this study. Since the excitation is applied in the plane including the stretching and chordwise motions, the stability of the stretching and chordwise motions can be simply guaranteed unless the oscillating frequency matches one of those natural frequencies. However, the stability of the flapwise motion cannot be easily checked, because the system of concern is a non-autonomous system with parametric excitation. Thus, the stability of the flapwise motion for the rotary oscillating cantilever beam is the main issue of this study. According to Ref. [22], when there is no applied force in the flapwise direction, the linear partial differential equation of flapwise motion is given by

$$\rho A\frac{\partial^2 w}{\partial t^2} + EI_y\frac{\partial^4 w}{\partial x^4} - \rho A\Omega^2\frac{\partial}{\partial x}\left\{\left[a(L-x) + \frac{1}{2}(L^2 - x^2)\right]\frac{\partial w}{\partial x}\right\} = 0, \tag{2}$$

where ρ is the mass density, A is the cross-sectional area, E is Young's modulus, and I_y is the area moments of inertia about the y-axis. The associate boundary conditions are given by

$$w = \frac{\partial w}{\partial x} = 0 \text{ at } x = 0, \quad \frac{\partial^2 w}{\partial x^2} = \frac{\partial^3 w}{\partial x^3} = 0, \quad \text{at } x = L. \tag{3}$$

It is assumed in this study that the rotary oscillating speed is prescribed by a harmonic function

$$\Omega(t) = \Omega_0 \sin \omega t, \tag{4}$$

where Ω_0 is the maximum angular speed and ω is the oscillating frequency.

To obtain more general results and conclusions, the equation needs to be transformed into a dimensionless form. For the purpose of the transformation, the following dimensionless variables need to be introduced:

$$w^* = \frac{w}{L}, \; t^* = \frac{t}{T}, \; x^* = \frac{x}{L}, \; a^* = \frac{a}{L}, \; \Omega_0^* = T\Omega_0, \; \omega^* = T\omega, \tag{5}$$

where

$$T = \sqrt{\frac{\rho A L^4}{E I_y}}. \tag{6}$$

Using these dimensionless variables, the equation of flapwise motion may be expressed in a dimensionless form. Dropping the asterisks from the dimensionless equation, the equation of the flapwise motion in the dimensionless form is given by

$$\frac{\partial^2 w}{\partial t^2} + \frac{\partial^4 w}{\partial x^4} - \Omega_0^2 \sin^2 \omega t \frac{\partial}{\partial x}\left\{\left[a(1-x) + \frac{1}{2}(1-x^2)\right]\frac{\partial w}{\partial x}\right\} = 0, \;\; \text{for } 0 \leqslant x \leqslant 1. \tag{7}$$

In order to find an approximated solution in a finite dimensional function space, the Galerkin method is used in this study. The solution of Eq. (7) is approximated by a series of comparison functions that satisfy both the essential and natural boundary conditions. The trial function for the approximated solution may be expressed as

$$w(t, x) = \sum_{n=1}^{N} u_n(t) W_n(x), \tag{8}$$

where N is the total number of comparison functions, $u_n(t)$ are unknown functions of time to be determined, and $W_n(x)$ are the eigenfunctions for the bending vibration of the stationary cantilever beam:

$$W_n(x) = \cosh \alpha_n x - \cos \alpha_n x - \frac{\sinh \alpha_n - \sin \alpha_n}{\cosh \alpha_n + \cos \alpha_n}(\sinh \alpha_n x - \sin \alpha_n x), \tag{9}$$

in which α_n are the roots of

$$\cos \alpha_n \cosh \alpha_n + 1 = 0. \tag{10}$$

The weighting function or the virtual function corresponding to Eq. (8) is given by

$$\bar{w}(t, x) = \sum_{n=1}^{N} \bar{u}_n(t) W_n(x), \tag{11}$$

where $\bar{u}_n(t)$ are arbitrary functions of time. It is noted that the comparison functions $W_n(x)$ satisfy the associated boundary conditions given by

$$w = \frac{\partial w}{\partial x} = 0 \quad \text{at } x = 0, \quad \frac{\partial^2 w}{\partial x^2} = \frac{\partial^3 w}{\partial x^3} = 0 \quad \text{at } x = 1. \tag{12}$$

Discretized equations of motion are determined by using Eqs. (8) and (11). Consider an equation obtained by substituting Eq. (8) into Eq. (7), multiplying the resultant equation by Eq. (11) and then integrating it over the domain $0 \leqslant x \leqslant 1$. If this equation is collected with respect to $\bar{u}_n(t)$, their coefficients provide the discretized equations since $\bar{u}_n(t)$ are arbitrary. The discretized equations of flapwise motion may then be expressed as

$$\ddot{u}_n + \omega_n^2 u_n + 4\varepsilon \sin^2 \omega t \sum_{m=1}^{N} f_{nm} u_m = 0 \quad \text{for } n = 1, 2, \cdots, N, \tag{13}$$

where the superposed dot represents the differentiation with respect to time; ω_n, ε and f_{nm} are given by

$$\omega_n = \left(\int_0^1 W_n \frac{\mathrm{d}^4 W_n}{\mathrm{d}x^4} \mathrm{d}x \right)^{1/2}, \quad \varepsilon = \frac{\Omega_0^2}{4},$$
$$f_{nm} = -\int_0^1 W_n \frac{\mathrm{d}}{\mathrm{d}x} \left\{ \left[a(1-x) + \tfrac{1}{2}(1-x^2) \right] \frac{\mathrm{d}W_m}{\mathrm{d}x} \right\} \mathrm{d}x. \tag{14}$$

Note that the dimensionless natural frequency of the stationary cantilever beam, ω_n, is equal to the square of the root of Eq. (10), α_n^2.

3. Method of multiple scales

The method of multiple scales is used to investigate the stability of the cantilever beam with rotary oscillation. Eq. (13) represents a typical parametrically excited system since the last term on the left-hand side of Eq. (13) is a periodic function of time. Following the method of multiple scales, the solution of Eq. (13) can be constructed by using a three-term approximation:

$$u_n(t;\, \varepsilon) \cong u_{n0}(T_0,\, T_1,\, T_2) + \varepsilon u_{n1}(T_0,\, T_1,\, T_2) + \varepsilon^2 u_{n2}(T_0,\, T_1,\, T_2), \tag{15}$$

where T_k are independent variables defined by

$$T_k = \varepsilon^k t \quad \text{for } k = 0,\, 1,\, 2. \tag{16}$$

Note that T_0 and T_1 are called the fast scale and the slow scale respectively. The fast scale is associated with changes occurring at the frequencies ω and ω_n, while the slow scale is associated with modulations in amplitudes and phases occurring at frequencies much lower than ω and ω_n.

Substituting Eq. (15) into Eq. (13) and collecting the resultant equation in terms of ε, the coefficients of ε^0, ε^1 and ε^2 provide the following partial differential equations:

$$D_0^2 u_{n0} + \omega_n^2 u_{n0} = 0, \tag{17}$$

$$D_0^2 u_{n1} + \omega_n^2 u_{n1} = -2D_0 D_1 u_{n0} + [\exp(2\mathrm{i}\omega T_0) + \exp(-2\mathrm{i}\omega T_0) - 2] \sum_{r=1}^{N} f_{nr} u_{r0}, \tag{18}$$

$$D_0^2 u_{n2} + \omega_n^2 u_{n2} = -2D_0 D_2 u_{n0} - D_1^2 u_{n0} - 2D_0 D_1 u_{n1} + [\exp(2\mathrm{i}\omega T_0) + \exp(-2\mathrm{i}\omega T_0) - 2] \sum_{r=1}^{N} f_{nr} u_{r1}, \tag{19}$$

where $\mathrm{i} = \sqrt{-1}$ and $D_k = \partial/\partial T_k$. It should be noted that the effective excitation frequency is 2ω in Eqs. (18) and (19), which is originated from $\sin^2\omega t$ of Eq. (13). This is different from other problems. For instance, the equation of motion for an axially oscillating cantilever beam has $\sin\omega t$ instead of $\sin^2\omega t$.

3.1. First order expansion

Related to the first order expansion, the transient curves, which divide stable and unstable regions, can be achieved by considering only u_{n0} and u_{n1} from Eq. (15). The general solution of Eq. (17) can be written in the form

$$u_{n0} = A_n(T_1, T_2)\exp(\mathrm{i}\omega_n T_0) + \mathrm{cc}, \tag{20}$$

where A_n are the complex amplitudes slowly varying with time and cc represents the complex conjugate of the preceding term. It should be noted that A_n are complex functions of only T_1 and T_2. Introduction of Eq. (20) into Eq. (18) leads to

$$D_0^2 u_{n1} + \omega_n^2 u_{n1} = -2\mathrm{i}\omega_n D_1 A_n \exp(\mathrm{i}\omega_n T_0) + \sum_{r=1}^{N} f_{nr} A_r \{\exp[\mathrm{i}(\omega_r + 2\omega)T_0] + \exp[\mathrm{i}(\omega_r - 2\omega)T_0] - 2\exp(\mathrm{i}\omega_r T_0)\} + \mathrm{cc}. \tag{21}$$

The complex functions A_n should be chosen to satisfy the conditions that u_{n1} are bounded. If the terms on the right-hand side of Eq. (21) have the excitation frequency ω_n, resonance occurs because the excitation frequency coincides with the natural frequency. These trouble terms, called the secular terms, should be eliminated from the right-hand side of Eq. (21).

Consider the case that ω is away from $(\omega_q \pm \omega_p)/2$ for all possible positive integer values of p and q. In this case the secular terms are eliminated when the following condition is satisfied:

$$\mathrm{i}\omega_n D_1 A_n + f_{nn} A_n = 0 \quad \text{for all } n. \tag{22}$$

The particular solutions of Eq. (21), when ω is away from $(\omega_q \pm \omega_p)/2$, are given by

$$u_{n1} = -\sum_{r=1}^{N} f_{nr} A_r \left\{ \frac{\exp[\mathrm{i}(\omega_r + 2\omega)T_0]}{(\omega_r + 2\omega)^2 - \omega_n^2} + \frac{\exp[\mathrm{i}(\omega_r - 2\omega)T_0]}{(\omega_r - 2\omega)^2 - \omega_n^2} \right\} + 2 \sum_{r=1, r\neq n}^{N} f_{nr} A_r \frac{\exp(\mathrm{i}\omega_r T_0)}{\omega_r^2 - \omega_n^2} + \mathrm{cc}. \tag{23}$$

Related to the stability criteria of the cantilever beam with rotary oscillation, the transient curves can be obtained from the conditions to eliminate the secular terms from approximate solutions. As shown in Table 1, there does not exist the case where ω is simultaneously near $(\omega_p + \omega_q)/2$ and $(\omega_l - \omega_k)/2$ for any integer values of p, q, l and k. In addition, since f_{pq} are symmetric, namely, $f_{pq} = f_{qp}$, as illustrated in Table 2, there is no unstable solution for the case

Table 1
Characteristic values α_n and the dimensionless natural frequencies ω_n of the stationary cantilever beam

n	α_n	ω_n
1	1.875104	3.516015
2	4.694091	22.034492
3	7.854757	61.697214
4	10.995541	120.901916
5	14.137168	199.859530
6	17.278760	298.555531
7	20.420352	416.990786
8	23.561944	555.165248
9	26.703538	713.078918
10	29.845130	890.731797

Table 2
Values of f_{nm} of the rotary oscillating cantilever beam when $\alpha = 0$

	m				
n	1	2	3	4	5
1	1.193336	−0.685855	−0.792379	−0.546413	−0.454075
2	−0.685855	6.478225	0.169408	−2.911851	−1.889167
3	−0.792379	0.169408	17.859520	3.274272	−6.154417
4	−0.546413	−2.911851	3.274272	36.055388	8.570157
5	−0.454075	−1.889167	−6.154417	8.570157	60.801076

where ω is near $(\omega_q - \omega_p)/2$. The reason is that unstable solutions occur when f_{pq} and f_{qp} have different signs [24]. Therefore, the transient curves need to be considered only when ω is near $(\omega_p + \omega_q)/2$.

When ω is near $(\omega_p + \omega_q)/2$, the nearness of ω to $(\omega_p + \omega_q)/2$ can be expressed by introducing a detuning parameter σ_1 defined by

$$\omega = \frac{1}{2}(\omega_p + \omega_q) + \frac{1}{2}\varepsilon\sigma_1. \tag{24}$$

After substituting Eq. (24) into Eq. (21), application of the conditions to eliminate the secular terms yields

$$2\mathrm{i}\omega_p D_1 A_p + 2f_{pp}A_p - f_{pq}\bar{A}_q \exp(\mathrm{i}\sigma_1 T_1) = 0, \tag{25}$$

$$2\mathrm{i}\omega_q D_1 A_q + 2f_{qq}A_q - f_{qp}\bar{A}_p \exp(\mathrm{i}\sigma_1 T_1) = 0, \tag{26}$$

where $\bar{A}_p$ and $\bar{A}_q$ are the complex conjugates of A_p and A_q. From the condition that non-trivial solutions of Eqs. (25) and (26) should be bounded, the transition curves, separating the $\varepsilon-\omega$ plane into stable and unstable regions, are obtained. The transition curves for the first order

approximation are given by

$$\omega = \frac{1}{2}(\omega_p + \omega_q) + \frac{1}{2}\varepsilon\left(\Gamma_{pq} \pm \sqrt{\Lambda_{pq}}\right), \tag{27}$$

where

$$\Gamma_{pq} = \frac{f_{pp}}{\omega_p} + \frac{f_{qq}}{\omega_q}, \quad \Lambda_{pq} = \frac{f_{pq}f_{qp}}{\omega_p\omega_q}. \tag{28}$$

3.2. Second order expansion

The transient curves for the second order expansion are obtained from the conditions that the solutions for u_{n0}, u_{n1} and u_{n2} should be bounded. Since the conditions to eliminate secular terms for u_{n0} and u_{n1} have been investigated in the previous section, the conditions for u_{n2} will be examined in this section. Introduction of Eqs. (20) and (23) into Eq. (19) leads to

$$\begin{aligned} D_0^2 u_{n2} + \omega_n^2 u_{n2} = & -(2\mathrm{i}\omega_n D_2 A_n + D_1^2 A_n)\exp(\mathrm{i}\omega_n T_0) \\ & - \sum_{r=1}^{N}\sum_{s=1}^{N} f_{nr}f_{rs}A_s \left\{ \frac{\exp[\mathrm{i}(\omega_s + 4\omega)T_0] - 2\exp[\mathrm{i}(\omega_s + 2\omega)T_0] + \exp(\mathrm{i}\omega_s T_0)}{(\omega_s + 2\omega)^2 - \omega_r^2} \right. \\ & \left. + \frac{\exp[\mathrm{i}(\omega_s - 4\omega)T_0] - 2\exp[\mathrm{i}(\omega_s - 2\omega)T_0] + \exp(\mathrm{i}\omega_s T_0)}{(\omega_s - 2\omega)^2 - \omega_r^2} \right\} \\ & + 2\sum_{r=1}^{N}\sum_{s=1, s\neq r}^{N} f_{nr}f_{rs}A_s \left\{ \frac{\exp[\mathrm{i}(\omega_s + 2\omega)T_0] + \exp[\mathrm{i}(\omega_s - 2\omega)T_0] - 2\exp(\mathrm{i}\omega_s T_0)}{\omega_s^2 - \omega_r^2} \right\} \\ & + 2\mathrm{i}\sum_{r=1}^{N} f_{nr}D_1 A_r \left\{ \frac{(\omega_r + 2\omega)\exp[\mathrm{i}(\omega_r + 2\omega)T_0]}{(\omega_r + 2\omega)^2 - \omega_n^2} + \frac{(\omega_r - 2\omega)\exp[\mathrm{i}(\omega_r - 2\omega)T_0]}{(\omega_r - 2\omega)^2 - \omega_n^2} \right\} \\ & - 4\mathrm{i}\sum_{r=1, r\neq n}^{N} f_{nr}D_1 A_r \frac{\omega_r \exp(\mathrm{i}\omega_r T_0)}{\omega_r^2 - \omega_n^2} + \mathrm{cc}. \end{aligned} \tag{29}$$

Since Eq. (23) is obtained when ω is far from $(\omega_q + \omega_p)/2$ and this equation is used to derive Eq. (29), under any resonance conditions the last two terms on the right-hand side of Eq. (29) do not produce the secular terms in u_{n2}. Therefore, these terms will not be considered in this section.

When ω is away from both $(\omega_q + \omega_p)/2$ and $(\omega_l + \omega_k)/4$ for all possible integer values of p, q, k and l, the secular terms are eliminated from u_{n2} if the following condition is satisfied:

$$2\mathrm{i}\omega_n D_2 A_n + D_1^2 A_n + 2\omega_n \chi_n A_n = 0, \tag{30}$$

where

$$\begin{aligned} \chi_n = & \frac{1}{2\omega_n}\sum_{r=1}^{N} f_{nr}f_{rn}\left[\frac{1}{(\omega_n + 2\omega)^2 - \omega_r^2} + \frac{1}{(\omega_n - 2\omega)^2 - \omega_r^2} \right] \\ & + \frac{2}{\omega_n}\sum_{r=1 r\neq n}^{N} \frac{f_{nr}f_{rn}}{\omega_n^2 - \omega_r^2}. \end{aligned} \tag{31}$$

Using Eqs. (22) and (30), it is easily proved that A_n is bounded. Therefore, the solution of u_{n2} is stable if ω is away from both $(\omega_q+\omega_p)/2$ and $(\omega_l+\omega_k)/4$.

Next, consider the case in which ω is near $(\omega_p+\omega_q)/2$. Using the detuning parameter defined by Eq. (24), the conditions that the secular terms are eliminated from u_{n2} may be expressed as

$$2\mathrm{i}\omega_p D_2 A_p + D_1^2 A_p + 2\omega_p \hat{\chi}_p A_p - 2\omega_p \eta_{pq} \bar{A}_q \exp(\mathrm{i}\sigma_1 T_1) = 0, \tag{32}$$

$$2\mathrm{i}\omega_q D_2 A_q + D_1^2 A_q + 2\omega_q \hat{\chi}_q A_q - 2\omega_q \eta_{qp} \bar{A}_p \exp(\mathrm{i}\sigma_1 T_1) = 0, \tag{33}$$

where

$$\hat{\chi}_p = \frac{1}{2\omega_p}\left[\sum_{r=1}^{N} \frac{f_{pr} f_{rp}}{(\omega_p+2\omega)^2-\omega_r^2} + \sum_{r=1, r\neq q}^{N} \frac{f_{pr} f_{rp}}{(\omega_p-2\omega)^2-\omega_r^2} + 4\sum_{r=1, r\neq p}^{N} \frac{f_{pr} f_{rp}}{\omega_p^2-\omega_r^2}\right], \tag{34}$$

$$\eta_{pq} = \frac{1}{2\omega_p}\left[\sum_{r=1, r\neq p}^{N} \frac{f_{pr} f_{rq}}{(\omega_q-2\omega)^2-\omega_r^2} + \sum_{r=1, r\neq q}^{N} \frac{f_{pr} f_{rq}}{\omega_q^2-\omega_r^2}\right]. \tag{35}$$

Note that A_p and A_q are functions of both T_1 and T_2. Hence, both the first and second order expansions should be considered simultaneously. For this purpose, combining Eqs. (25) and (32) as well as Eqs. (26) and (33), the following equations may be obtained:

$$2\mathrm{i}\omega_p \frac{\mathrm{d}A_p}{\mathrm{d}t} + \left[2\varepsilon f_{pp} + \varepsilon^2\left(\frac{1}{4}\Lambda_{pq} - \frac{f_{pp}^2}{\omega_p^2} + 2\omega_p\hat{\chi}_p\right)\right] A_p + \left[-\varepsilon f_{pq} + \varepsilon^2\left(\frac{f_{pp}f_{pq}}{2\omega_p^2} - \frac{f_{qq}f_{pq}}{2\omega_p\omega_q} - 2\omega_p\eta_{pq} + \frac{\sigma_1 f_{pq}}{2\omega_p}\right)\right]\bar{A}_q \exp(\mathrm{i}\varepsilon\sigma_1 t) = 0, \tag{36}$$

$$2\mathrm{i}\omega_q \frac{\mathrm{d}A_q}{\mathrm{d}t} + \left[2\varepsilon f_{qq} + \varepsilon^2\left(\frac{1}{4}\Lambda_{pq} - \frac{f_{qq}^2}{\omega_q^2} + 2\omega_q\hat{\chi}_q\right)\right] A_q + \left[-\varepsilon f_{qp} + \varepsilon^2\left(\frac{f_{qq}f_{qp}}{2\omega_q^2} - \frac{f_{pp}f_{qp}}{2\omega_p\omega_q} - 2\omega_q\eta_{qp} + \frac{\sigma_1 f_{qp}}{2\omega_q}\right)\right]\bar{A}_p \exp(\mathrm{i}\varepsilon\sigma_1 t) = 0. \tag{37}$$

For a similar reason as before, Eqs. (36) and (37) should have non-trivial solutions whose magnitudes are bounded. From theses conditions, the transient curves can be determined. The transient curves of the second order expansion when ω is near $(\omega_p+\omega_q)/2$ may be expressed by

$$\omega = \frac{1}{2}(\omega_p+\omega_q) + \frac{1}{2}\varepsilon\left(\Gamma_{pq} \pm \sqrt{\Lambda_{pq}}\right) - \frac{1}{16}\varepsilon^2 \left[4\Phi_{pq} + \Lambda_{pq}\left(\frac{1}{\omega_p}+\frac{1}{\omega_q}\right) - 8\left(\hat{\chi}_p+\hat{\chi}_q\right) \pm 4\sqrt{\Lambda_{pq}}\left(\Pi_{pq} - 2\frac{\omega_p}{f_{pq}}\eta_{pq} - 2\frac{\omega_q}{f_{qp}}\eta_{qp}\right)\right], \tag{38}$$

where

$$\Phi_{pq} = \frac{f_{pp}^2}{\omega_p^3} + \frac{f_{qq}^2}{\omega_q^3}, \qquad \Pi_{pq} = \frac{f_{pp}}{\omega_p^2} + \frac{f_{qq}}{\omega_q^2}. \tag{39}$$

Finally, consider the case that ω is near $(\omega_p + \omega_q)/4$. Similarly to Eq. (24), a detuning parameter σ_2 is used, which is defined by

$$\omega = \frac{1}{4}(\omega_p + \omega_q) + \frac{1}{4}\varepsilon\sigma_2. \tag{40}$$

After substituting Eq. (40) into Eq. (29), from the conditions that the secular terms are eliminated, the following equations can be obtained:

$$2\mathrm{i}\omega_p D_2 A_p + D_1^2 A_p + 2\omega_p \chi_p A_p + 2\omega_p \mu_{pq} \bar{A}_q \exp(\mathrm{i}\sigma_2 T_1) = 0, \tag{41}$$

$$2\mathrm{i}\omega_q D_2 A_q + D_1^2 A_q + 2\omega_q \chi_q A_q + 2\omega_q \mu_{qp} \bar{A}_p \exp(\mathrm{i}\sigma_2 T_1) = 0. \tag{42}$$

where

$$\mu_{pq} = \frac{1}{2\omega_p} \sum_{r=1}^{N} \frac{f_{pr} f_{qr}}{(\omega_q - 2\omega)^2 - \omega_r^2}. \tag{43}$$

As pointed out in the previous paragraph, since A_p and A_q are functions of both T_1 and T_2, both the first and second order expansions should also be considered simultaneously. Combining Eqs. (25) and (41) results in

$$2\mathrm{i}\omega_p \frac{\mathrm{d}A_p}{\mathrm{d}t} + \left[2\varepsilon f_{pp} + \varepsilon^2 \left(2\omega_p \chi_p - \frac{f_{pp}^2}{\omega_p^2}\right)\right] A_p + 2\varepsilon^2 \omega_p \mu_{pq} \bar{A}_q \exp(\mathrm{i}\varepsilon\sigma_2 t) = 0, \tag{44}$$

while combining Eqs. (26) and (42) results in

$$2\mathrm{i}\omega_q \frac{\mathrm{d}A_q}{\mathrm{d}t} + \left[2\varepsilon f_{qq} + \varepsilon^2 \left(2\omega_q \chi_q - \frac{f_{qq}^2}{\omega_q^2}\right)\right] A_q + 2\varepsilon^2 \omega_q \mu_{qp} \bar{A}_p \exp(\mathrm{i}\varepsilon\sigma_2 t) = 0. \tag{45}$$

From the conditions that Eqs. (44) and (45) have bounded non-trivial solutions, the transient curves, when ω is near $(\omega_p + \omega_q)/4$, may be expressed as

$$\omega = \frac{1}{4}(\omega_p + \omega_q) + \frac{1}{4}\varepsilon\Gamma_{pq} + \frac{1}{8}\varepsilon^2 \left[2(\chi_p + \chi_q) - \Phi_{pq} \pm 4\sqrt{\mu_{pq}\mu_{qp}}\right]. \tag{46}$$

Although, in general cases, the second order transient curves may exist around $\omega \cong (\omega_p - \omega_q)/4$, such is not true for the cantilever beam with rotary oscillation.

4. Stability analysis

The stability of a cantilever beam with rotary oscillation is analyzed for variations of the oscillating frequency and the maximum angular speed. For simplicity, the hub radius a is assumed as zero and discussion of the first order expansion is omitted from this paper. In order to obtain the transient curves and time responses, the dimensionless partial differential Eq. (7) is discretized into 10 ordinary differential equations. In other words, N in Eq. (13) is selected as 10. The transient curves obtained from the second order expansion are plotted in Fig. 2 for the variations of ω/ω_1 and ε/ω_1^2. In Fig. 2, the hatched parts represent the unstable region and the remaining part represents the stable region. The boundaries of the unstable regions for $\omega = \omega_1$, $(\omega_1 + \omega_2)/2$ and ω_2 are defined by Eq. (38) while those of the unstable regions for $\omega = \omega_1/2$, $(\omega_1 + \omega_2)/4$,

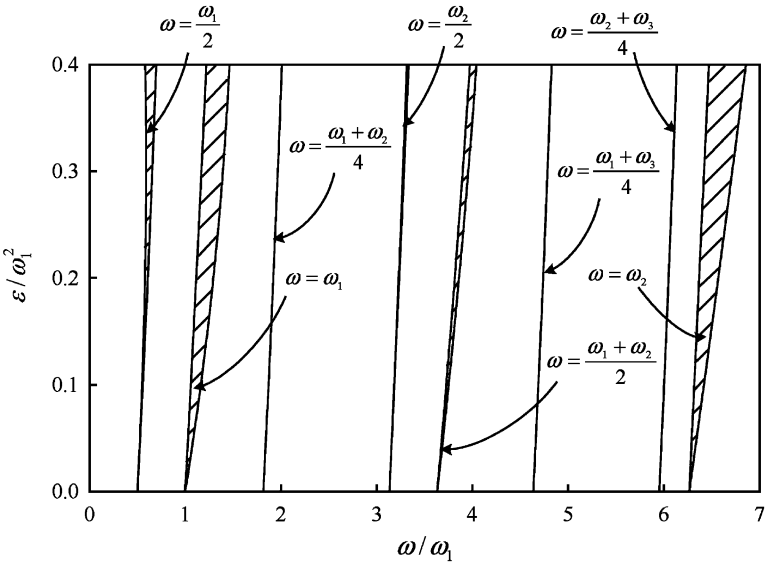

Fig. 2. Stability plot of the second order expansion for the cantilever beam with rotary oscillation.

$\omega_2/2$, $(\omega_1 + \omega_3)/4$ and $(\omega_2 + \omega_3)/4$ are defined by Eq. (46). It is interesting to observe that the unstable regions near $\omega = (\omega_p + \omega_q)/2$ are relatively larger than those near $\omega = (\omega_p + \omega_q)/4$. In fact, the unstable regions obtained from the first order expansion are not much different from the unstable regions near $\omega = (\omega_p + \omega_q)/2$ of Fig. 2. It is also seen in Fig. 2 that the unstable regions become large as the maximum angular speed, i.e., ε/ω_1^2 increases.

The results of the stability analysis are verified by investigating the time responses. Applying the generalized-α time integration method [25] to the discretized equations given by Eq. (13), the time responses for the flapwise displacement are computed at the free end of the beam. The beam is initially deformed by a static force at the free end. The displacement at the free end is 0.01 and the beam is released from rest. The algorithmic parameters of the generalized-α method are selected for the case without numerical dissipation and the time step size for numerical integration is 0.01. Time responses are computed for 12 points marked in Fig. 3.

First, the time responses when ω is near $(\omega_p + \omega_q)/2$ are examined. For three points that are located at $\omega \cong \omega_1$, time responses are computed and presented in Fig. 4. The co-ordinates of points A_1, A_2 and A_3 in Fig. 3 are (1.0, 0.35), (1.33, 0.2) and (1.33, 0.35). Points A_1 and A_2 are in the stable region but point A_3 is in the unstable region, as shown in Fig. 3. Fig. 4(a) demonstrates that the time response for point A_1 is bounded by a limited value, even though the excitation frequency is equal to the first natural frequency of the stationary cantilever, namely, ω_1. When the oscillation frequency and the maximum angular speed correspond to point A_2, the time response, as shown in Fig. 4(b), has frequency modulation and it is also bounded. However, for point A_3, which is inside the unstable region, the amplitude of the time response increases with time, as illustrated in Fig. 4(c). Therefore, it is verified that the stability results of Fig. 3 well agree with the behaviours of the time responses of Fig. 4. When the oscillating frequency ω is near $(\omega_1 + \omega_2)/2$, time responses are also examined for points B_1(3.68, 0.2) and B_2(3.83, 0.2). Since the time responses of

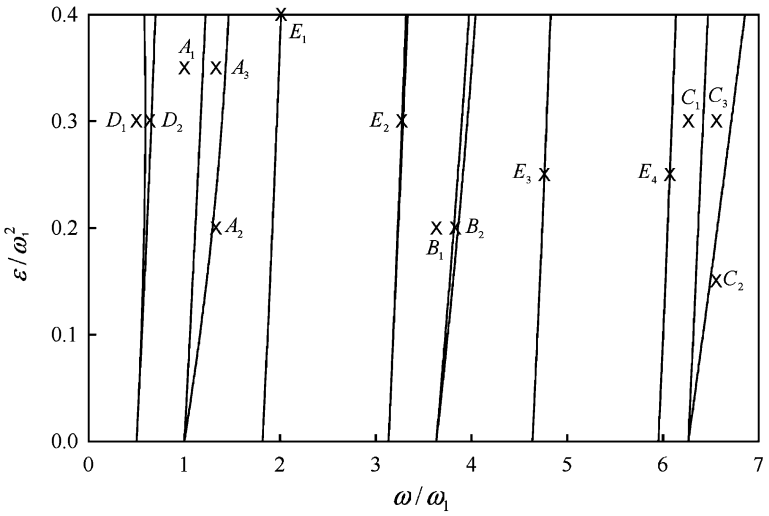

Fig. 3. Points selected to verify the stability of the cantilever beam with rotary oscillation.

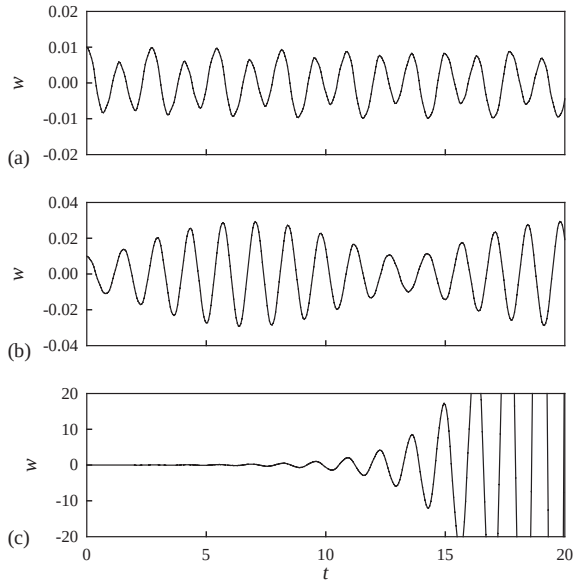

Fig. 4. Time responses of the cantilever beam with rotary oscillation for (a) point $A_1(1.0, 0.35)$, (b) point $A_2(1.33, 0.2)$ and (c) point $A_3(1.33, 0.35)$.

Fig. 5 are bounded and unbounded for B_1 and B_2, respectively, the stability analysis near $\omega = (\omega_1 + \omega_2)/2$ is reliable. Similarly, the stability can be verified in the neighbourhood of $\omega = \omega_2$. Fig. 6 shows time responses for points $C_1(6.2669, 0.3)$, $C_2(6.56, 0.15)$ and $C_3(6.56, 0.3)$ of Fig. 3. Because the time responses for points C_1 and C_2 are bounded and the response for point C_3 is unbounded, the behaviours of the time responses well coincide to the stability results of Fig. 2.

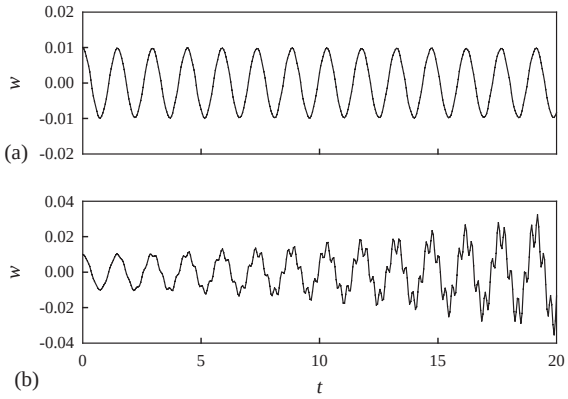

Fig. 5. Time responses of the cantilever beam with rotary oscillation for (a) point $B_1(3.63, 0.2)$ and (b) point $B_2(3.83, 0.2)$.

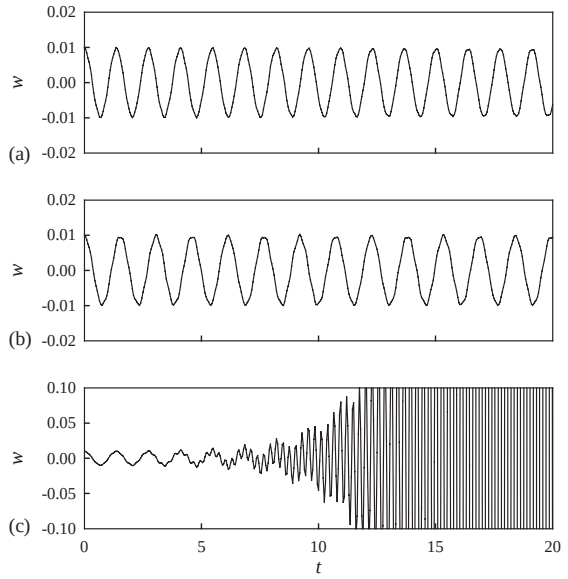

Fig. 6. Time responses of the cantilever beam with rotary oscillation for (a) point $C_1(6.2669, 0.3)$, (b) point $C_2(6.56,\ 0.15)$ and (c) point $C_3(6.56, 0.3)$.

Next, the stability results around $\omega = (\omega_p + \omega_q)/4$ are investigated. Consider points $D_1(0.5, 0.3)$ and $D_2(0.64, 0.3)$ of Fig. 3, which are located near $\omega = \omega_1/2$. These two points are in the stable and unstable regions, respectively. Time responses computed at points D_1 and D_2, plotted in Fig. 7, show bounded and unbounded responses. Hence, it can be said that the stability results near $\omega = \omega_1/2$ are validated. Consider the case that the oscillating frequencies are near $\omega = (\omega_1 + \omega_2)/4$ and $\omega = \omega_2/2$. Points $E_1(2.011, 0.4)$ and $E_2(3.27, 0.3)$ are in the unstable regions of Fig. 3. As expected, time responses corresponding to points E_1 and E_2 increase with time as presented in Fig. 8. In contrast to the other time responses, the vibration amplitudes very slowly

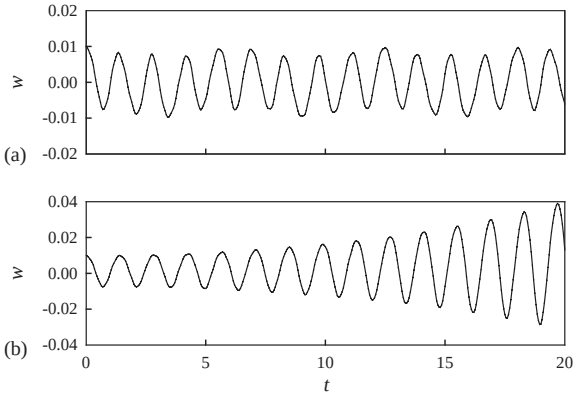

Fig. 7. Time responses of the cantilever beam with rotary oscillation for (a) point $D_1(0.5, 0.3)$ and (b) point $D_2(0.64, 0.3)$.

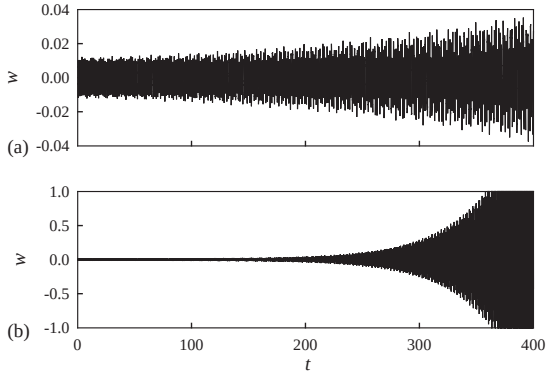

Fig. 8. Time responses of the cantilever beam with rotary oscillation for (a) point $E_1(2.011, 0.4)$ and (b) point $E_2(3.27, 0.3)$.

increase with time. However, the unstable regions near $\omega = (\omega_1 + \omega_3)/4$ and $\omega = (\omega_2 + \omega_3)/4$ are too narrow to find a point at which a time response becomes unstable. Numerical errors in the computed natural frequencies ω_n of Table 1 and the values f_{nm} of Table 2 may make it difficult to find a point where a time response is unbounded. In fact, even if points $E_3(4.763101039, 0.25)$ and $E_4(6.072859571, 0.25)$ are inside numerically computed stable regions, time responses corresponding to these points do not exhibit unstable behaviours even over a very long duration, e.g., 1000.

Finally, it is interesting to discuss the unstable time responses in more detail. Note that the unstable responses when $\omega \approx \omega_p$ grow dramatically with time, as shown in Figs. 4(c) and 6(c), while the unstable responses when $\omega \approx \omega_p/2$, $(\omega_p + \omega_q)/2$ or $(\omega_p + \omega_q)/4$ grow gradually, as shown in Figs. 5(b), 7(b) and 8. This implies that only the primary resonance corresponding to $\omega \approx \omega_p$ possesses a rapid increase in amplitude. The secondary resonance when $\omega \approx \omega_p/2$ and the combination resonance when $\omega \approx (\omega_p + \omega_q)/2$ or $(\omega_p + \omega_q)/4$ show a slow increase in amplitude. One more interesting phenomenon can be observed in Figs. 5(b) and 6(c). The time responses

shown in these figures have two main frequency components: one is near ω_1 and the other is near ω_2. Comparison of these frequencies yields the fact that ω_2 is approximately three times of ω_1, that is, $\omega_2 \approx 3\omega_1$. Therefore, it may be concluded that the internal resonance occurs in the responses plotted in Figs. 5(b) and 6(c).

5. Conclusions

The dynamic stability of the flapwise motion is analyzed for the cantilever beam with rotary oscillation. To describe the flapwise motion, this study adopts the linear partial differential equation with parametric excitation, which is derived by using stretch deformation instead of the conventional longitudinal deformation. After this partial differential equation is transformed to a dimensionless equation, it is discretized by the Galerkin method. By applying the method of multiple scales to the discretized equations, the stability plot is obtained for the variations of the oscillating frequency and the maximum angular speed, and then the stability of the flapwise motion is investigated. The results of the stability analysis are verified by time responses computed at several points on the stability plot.

The results of the stability analysis can be summarized as follows:

(1) The unstable regions exist when the oscillating frequency ω is near $(\omega_p + \omega_q)/2$ or $(\omega_p + \omega_q)/4$, where ω_p and ω_q are the natural frequencies of the stationary cantilever beam and p and q are positive integers.
(2) The unstable regions become large as the maximum angular speed increases.
(3) The unstable regions when $\omega \cong (\omega_p + \omega_q)/2$ are relatively larger than those when $\omega \cong (\omega_p + \omega_q)/4$.
(4) The unstable regions when $\omega \cong (\omega_1 + \omega_3)/2$ or $\omega \cong (\omega_2 + \omega_3)/2$ are too narrow to find points at which time responses become unstable.

Acknowledgements

This study was supported by the Brain Korea 21 Project of the Ministry of Education and the Center of Innovative Design Optimization Technology (ERC of Korea Science and Engineering Foundation). These supports are gratefully acknowledged.

References

[1] M. Faraday, On a peculiar class of acoustical figures and on certain forms assumed by a group of particles upon vibrating elastic surfaces, *Philosophical Transactions of the Royal Society* 121 (1831) 299–318.
[2] E. Mathieu, Memoire sur ie mouvement vibratoire d'une membrane de forme elliptique, *Journal of Mathematics* 13 (1868) 137–203.
[3] G. Hill, On the part of the lunar perigee which is a function of the mean motions of the Sun and Moon, *Acta Mathematica* 8 (1886) 1–36.

[4] A. Stephenson, On a new type of dynamical stability, *Memoirs and Proceedings of the Manchester Literary and Philosophical Society* 52 (1908) 1907–1908.
[5] A. Andronov, M.A. Leontovich, On the vibrations of systems with periodically varying parameters, *Zhurnal Russkago Fiziko-Khimicheskago Obshchestva* 59 (1927) 429–443.
[6] C. Hsu, On the parametric excitation of a dynamic system having multiple degrees of freedom, *Journal of Applied Mechanics* 30 (1963) 367–372.
[7] K. Lindh, P. Likins, Infinite determinant methods for stability analysis of periodic-coefficient differential equations, *American Institute of Aeronautics and Astronautics Journal* 8 (1970) 680–686.
[8] F. Fu, S. Nemat-Nasser, Stability of solution of systems of linear-differential equations with harmonic coefficients, *American Institute of Aeronautics and Astronautics Journal* 10 (1973) 30–36.
[9] C. Hsu, On approximating a general linear periodic system, *Journal of Mathematical Analysis and Application* 45 (1974) 234–251.
[10] A.H. Nayfeh, D.T. Mook, Parametrically excitations of linear systems having many degrees of freedom, *Journal of Acoustical Society of America* 62 (1977) 375–381.
[11] J.A. Wickert, C.D. Mote, Response and discretization methods for axially moving materials, *American Society of Mechanical Engineers Applied Mechanics Reviews* 44 (1991) 279–284.
[12] J.A. Wickert, Transient vibration of gyroscopic systems with unsteady superposed motion, *Journal of Sound and Vibration* 195 (1996) 797–807.
[13] M. Pakdemirli, A.G. Ulsoy, Stability analysis of an axially accelerating string, *Journal of Sound and Vibration* 203 (1997) 815–832.
[14] S.H. Hyun, H.H. Yoo, Dynamic modeling and stability analysis of axially oscillating cantilever beams, *Journal of Sound and Vibration* 228 (1999) 543–558.
[15] C. Lin, L. Chen, Dynamic stability of rotating composite beams with a viscoelastic core, *Composite Structures* 58 (2002) 185–194.
[16] T.H. Tan, H.P. Lee, G.S.B. Leng, Dynamic stability of a radially rotating beam subjected to base excitation, *Computer Methods in Applied Mechanics and Engineering* 146 (1997) 265–279.
[17] T.H. Tan, H.P. Lee, G.S.B. Leng, Parametric instability of spinning pretwisted beams subjected to spin speed perturbation, *Computer Methods in Applied Mechanics and Engineering* 148 (1997) 139–163.
[18] H.H. Yoo, R.R. Ryan, R.A. Scott, Dynamics of flexible beams undergoing overall motion, *Journal of Sound and Vibration* 181 (1995) 261–278.
[19] H. Frisch, A vector-dyadic development of the equations of motion for N-coupled flexible bodies and point masses, NASA TND-8047, 1975.
[20] J. Ho, Direct path method for flexible multibody spacecraft dynamics, *Journal of Spacecraft and Rockets* 14 (1997) 102–110.
[21] C. Bodley, A. Devers, A, Park, H. Frisch, A digital computer program for the dynamic interaction, simulation of controls and structure, NASA TP-1219.
[22] J. Chung, H.H. Yoo, Dynamic analysis of a rotating cantilever beam by using the finite element method, *Journal of Sound and Vibration* 249 (2002) 147–164.
[23] A.H. Nayfeh, *Perturbation Methods*, Wiley, New York, 1973.
[24] A.H. Nayfeh, D.T. Mook, *Nonlinear Oscillations*, Wiley, New York, 1979.
[25] J. Chung, G.M. Hulbert, A time integration algorithm for structural dynamics with improved numerical dissipation: the generalized-α method, *American Society of Mechanical Engineers Journal of Applied Mechanics* 60 (1993) 371-375.